# Distributed Virtual Inertia Based Control of Multiple Photovoltaic Systems in Autonomous Microgrid

Won-Sang Im, *Member, IEEE,* Cheng Wang, *Student Member, IEEE,* Wenxin Liu, *Senior Member, IEEE,* Liming Liu, *Senior Member, IEEE,* and Jang-Mok Kim, *Member, IEEE*

***Abstract*—The large inertia of a traditional power system slows down system's frequency response but also allows decent time for controlling the system. Since an autonomous renewable microgrid usually has much smaller inertia, the control system must be very fast and accurate to fight against the small inertia and uncertainties. To reduce the demanding requirements on control, this paper proposes to increase the inertia of photovoltaic (PV) system through inertia emulation. The inertia emulation is realized by controlling the charging/discharging of the direct current (DC)-link capacitor over a certain range and adjusting the PV generation when it is feasible and/or necessary. By well designing the inertia, the DC-link capacitor parameters and the control range, the negative impact of inertia emulation on energy efficiency can be reduced. The proposed algorithm can be integrated with distributed generation setting algorithms to improve dynamic performance and lower implementation requirements. Simulation studies demonstrate the effectiveness of the proposed solution.**

***Index Terms*—Inertia emulation, microgrid, photovoltaic system, renewable energy, voltage source converter.**

## I. Introduction

MICROGRID can be defined as a cluster of loads and distributed energy resource (DER) units, serviced by a distribution system and can operate autonomously without connecting to power grid. The microgrid concept is a big step towards solving the controllability problems of distributed resources. A microgrid is a quite appealing alternative for overcoming the challenges of integrating DER units, including renewable energy sources, into power systems etc. [1]−[4].

For a microgrid to work autonomously, it must maintain its own supply-demand balance. If supply does not match demand, the grid frequency will change at a rate determined by the total microgrid inertia coefficient that is decided by the overall spinning kinetic energy in the microgrid. Since inertia stands for the sensitivity of frequency to supply-demand mismatch, it plays an important role as primary reserve [5]−[7]. However, the inertia of autonomous microgrids under high renewable penetration is usually very small due to the integration of large number of power electronic interfaced distributed generators [8], [9].

Unlike doubly-fed induction generators (DFIG) that still possess reduced inertia, the fully voltage source converter (VSC) interfaced photovoltaic (PV) system does not have any kinetic energy thus does not contribute any inertia to the power system. For autonomous microgrids under high PV penetration, the small inertia of microgrid makes the system very hard to control. Developing brand new microgrid control solutions which are fast and accurate, is very challenging and still has a long way to go. During this stage, it is still necessary to intentionally increase the inertia of the microgrids to lower control difficulty. In this way, the solutions that have proven being successful for large-scale power systems can be introduced to autonomous microgrid.

Inertia utilization and inertia emulation of renewable energy resources have been studied in recent years. In [10]−[13], wind generator's rotor inertia is utilized to counteract grid frequency fluctuations. One disadvantage with these methods is that even small grid frequency changes steadily affect the action of the wind turbine's blade and the recovery of rotor speed can be difficult after large frequency deviations. In [14], DC-link capacitor energy is used for inertia emulation in VSC-HVDC transmission system for wind farms. If the grid frequency changes, DC-link voltage reference of VSC is adjusted to inject or absorb active power for suppressing frequency fluctuation. The advantage of this control method is that it has no impact on the rectifier connected to wind farms. To emulate large inertia, this method requires big capacitance and wide range DC-link voltage. Also, high DC-link voltage should be set to satisfy the wide DC-link voltage margin, which will cause more switching loss and noise and require stronger filters. Using additional energy storage (ES) can address the disadvantages effectively but will increase cost [15].

For autonomous microgrids, deloading of the renewable generators (RGs) becomes necessary under redundant renewable generation. To realize frequency stabilization or supply demand balance, the multiple RGs must be well coordinated. In authors previous papers [16], [17], two fully distributed algorithms are presented for this purpose. The concept is to synchronize all utilization levels of multiple RGs to the desired level. In [16], a consensus based information discovery algo-

Manuscript received October 12, 2015; accepted May 25, 2016. Recommended by Associate Editor Qinmin Yang. *(Corresponding author: Won-Sang Im.)*

Citation: W. -S. Im, C. Wang, W. X. Liu, L. M. Liu, and J. -M. Kim, "Distributed virtual inertia based control of multiple photovoltaic systems in autonomous microgrid," *IEEE/CAA J. of Autom. Sinica*, vol. 4, no. 3, pp. 512−519, Jul. 2017.

W. -S. Im, C. Wang, and W. X. Liu are with Lehigh University, Bethlehem PA 18015, USA (e-mail: won42@pusan.ac.kr; chwang925@gmail.com; wliu@lehigh.edu).

L. M. Liu is with ABB Inc., Raleigh NC 27606, USA (e-mail: liming.liu@us.abb.com).

J. -M. Kim is with Pusan National University, Busan 46241, Korea (e-mail: jmok@pusan.ac.kr).

Color versions of one or more of the figures in this paper are available online at http://ieeexplore.ieee.org.

Digital Object Identifier 10.1109/JAS.2016.7510031

rithm is presented to calculate the desired utilization level. In [17], the coordination problem is formulated as an optimization problem and solved by distributed subgradient algorithm. For both algorithms, the generation references of the RGs are updated periodically. To achieve good dynamic performance the updating interval of the generation reference must be small enough and well-tuned. For large and complicated microgrids, the requirements might become hard to satisfy. The difficulties are mainly due to the fact that transient performance is not considered during problem formulation.

The objective of the paper is to improve transient control performance of autonomous renewable microgrid and lower the implementation difficulties of the distributed deloading algorithms [16], [17]. The objectives are realized by increasing the inertia of PV systems to emulate traditional synchronous generators (SGs). For inertia emulation, the overall generation must be flexibly adjusted based on grid frequency. To minimize the impact on energy efficiency, the first choice is to well utilize the ES components in the PV systems, i.e., the DC-link capacitor, just like the way in [14]. Since the charging and discharging of the DC-link capacitor does not have any impact on PV generation, long-term energy efficiency is not affected. As mentioned earlier, the amount of power that can be adjusted by the DC-link capacitor is limited. If the requirement for inertia emulation is beyond certain limit, the PV array's output must be adjusted higher or lower. If renewable generation is more than needed, this adjustment has no impact on energy efficiency. Even when energy efficiency is a big concern, we might need to compromise it in exchange for better stability and transient performance. Thus, the proposed solution is practical and reasonable, as demonstrated through simulations with autonomous microgrids with multiple RGs.

The rest paper is organized as follows. Section II introduces the virtual inertia concept of PV system. Section III introduces how virtual inertia can be emulated through DC-link voltage control and PV array generation adjustment. Simulation results with a multiple-RG microgrid are presented in Section IV. Finally, the concluding remarks are provided in Section V.

## II. Virtual Inertia of PV System

In traditional power systems, supply-demand imbalance changes system frequency at a rate determined by the total system inertia, which is given by

$$\Delta P = \frac{2\Sigma H}{f_0} \cdot \frac{df}{dt} \ (\mathrm{pu}) \tag{1}$$

where $\Delta P$ is the active power supply-demand imbalance, $\Sigma H$ is the total inertia coefficient, $f_0$ is the nominal frequency, and $f$ presents the grid frequency.

The inertia in a power system mainly comes from the SGs. The inertia coefficient of a SG, $H_{\mathrm{SG}}$, is given as (2).

$$H_{\mathrm{SG}} = \frac{W_k}{S_{\mathrm{SG}}} \tag{2}$$

where $W_k$ presents the kinetic energy stored in the rotating rotor and $S_{\mathrm{SG}}$ is generator rated power capability.

To increase the overall inertia of the autonomous microgrid, it is important to increase the inertia of the VSC interfaced RG, especially the zero-inertia PV systems. Fig. 1 shows the topology of a typical PV system that consists of a PV array, a DC-DC boost converter, a DC-link capacitor, and a VSC. The PV array generates DC power, which is boosted to meet the grid voltage requirement. The DC-link capacitor is mainly used for voltage stabilization and decoupling. Finally, the VSC is used to convert DC to AC and to meet the grid code.

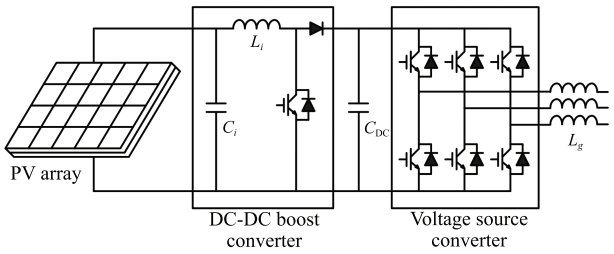


Fig. 1. Topology of a PV system.

To emulate the inertia of SG, the virtual inertia coefficient of a PV system can be defined in a similar way as (3).

$$H_{\mathrm{PV}} = \frac{W_E}{S_{\mathrm{PV}}} \tag{3}$$

where $W_E$ is the kinetic energy to emulate and $S_{\mathrm{PV}}$ is the PV system's rated power capacity.

Similar to that of SG, The frequency dynamics of the PV system during inertia emulation can be given by

$$\Delta P_{\mathrm{IE}} = \frac{2H_{\mathrm{PV}}}{f_0} \frac{df}{dt} \tag{4}$$

where $\Delta P_{\mathrm{IE}}$ is the change of active power generation of the PV system for inertia emulation.

According to (4), the inertia of $H_{\mathrm{PV}}$ can be emulated if the generation of PV system can be properly adjusted. During implementation, a generator periodically receives generation reference from upper-level controller, either centralized or distributed. Operational constraints, such as energy efficiency, supply-demand balance, and other constraints, can be addressed during generation references setting. Once the generation reference is received, it will be deployed immediately and then adjusted according to (5) until a new generation reference is delivered.

$$P_G = P_{G0} - \Delta P_{\mathrm{IE}} \tag{5}$$

where $P_{G0} = P_{\mathrm{PV0}}$ is the generation setting from upper level controller and $P_G$ is the updated generation setting due to inertia emulation.

From (5), one can see that if there is no inertia emulation ($\Delta P_{\mathrm{IE}} = 0$), there is no generation adjustment $P_G = P_{G0}$. If the grid frequency increases (rotational speed of the emulated SG increases), more kinetic energy will be stored for inertia emulation. By subtracting the power for inertia emulation ($\Delta P_{\mathrm{IE}}$), the PV generation will be reduced. Reduced generation will help reducing system frequency. The opposite scenario can be explained in a similar way.

The concept can be better understood by comparing it with the hierarchical control scheme in traditional power systems. $\Delta P_{\mathrm{IE}}$ is like the decentralized droop or local controls that are myopic. To correct the semi-steady control deviation

and address other system level considerations, upper-level economic dispatch and automatic generation control will be activated periodically. Here, it is assumed that $P_{G0}$ is a good control setting for the instant of time it is delivered to the PV system. The idea is like adding a differential adjustment to generation reference. In the following section, we will discuss how to realize inertia emulation.

## III. Inertia Emulation of PV System

Before continuing our discussion, it should be noted that the virtual inertia based deloading control is just one mode of control. During generation shortage, all PV systems should work at maximum power point tracking (MPPT) mode. If renewable generation itself is more than demand and/or frequency regulation becomes more important, some or all of the PV systems can work at the inertia emulation mode. Even though energy efficiency becomes secondary under this mode, it is still important to maintain the energy efficiency as much as possible.

One way is to fully utilize the ES unit of the PV system, i.e., the DC-link capacitor. Since charging and discharging of the capacitor does not affect the MPPT control of PV array, energy efficiency in the long run is not impacted. Since the size and voltage range of the capacitor are limited, its contribution to inertia emulation is limited. If the emulated inertia or the change of frequency is beyond the capability of DC-link capacitor, the generation from the PV array has to be adjusted. Reducing PV array generation might compromise energy efficiency. In above two-step solution for inertia emulation, the capacitor control is the first choice and PV generation adjustment is the second choice.

The overall generation adjustment for inertia emulation is implemented according to (6). The implementation details are introduced as follows.

$$\Delta P_{\rm IE} = \Delta P_C + \Delta P_{\rm PV} \tag{6}$$

where $\Delta P_C$ is the contribution to inertia emulation from DC link voltage control and $\Delta P_{\rm PV}$ is the contribution from PV array generation adjustment.

### A. Inertia Emulation Through DC-link Voltage Control

DC-link capacitors are used to maintain the DC-link voltage and alleviate voltage ripple. The capacity is determined by permission rate of the voltage ripple, voltage level, switching frequency of power electronics, etc. The PV system generally has small DC-link capacity because of the constraints on cost and size. Hence, the capacitor itself is only capable of emulating small inertia. However, this capacitor is useful for small oscillation damping if properly controlled.

The energy stored in the DC-link capacitor ($W_C$) is given by

$$W_C = \frac{1}{2} C_{\rm DC} V_{\rm DC}^2 \tag{7}$$

where $C_{\rm DC}$ is the capacitance of the DC-link capacitor and $V_{\rm DC}$ is the DC-link voltage.

The power of the DC-link capacitor in per unit can be presented by (8), which means the change of the DC-link voltage can generate power.

$$\Delta P_C = \frac{C_{\rm DC} V_{\rm DC}}{S_{\rm PV}} \cdot \frac{dV_{\rm DC}}{dt}. \tag{8}$$

Conventionally, the control reference for DC-link voltage in VSC is set to a fixed value. Thus, the DC-link capacitor's capability is not utilized. In [14], it is shown that DC-link capacitor's energy can be used for virtual inertia emulation if variable DC-link voltage reference ($V_{\rm DC}^*$) defined as (9) is introduced.

$$V_{\rm DC}^* = \sqrt{\frac{4 S_{\rm PV} H_{\rm PV}}{C_{\rm DC} f_0} f - \frac{4 S_{\rm PV} H_{\rm PV}}{C_{\rm DC}} + V_{\rm DC0}^2} \tag{9}$$

where $V_{\rm DC0}$ presents the nominal DC-link voltage.

From (9), one can see that the $V_{\rm DC}^*$ is a nonlinear function of system frequency $f$. Setting of $V_{\rm DC}^*$ is also related to other rating and parameters of the PV system and the inertia to emulate. Fig. 2 shows the relationships between $V_{\rm DC}^*$ and $f$ for different $C_{\rm DC}$ and $H_{\rm PV}$, $H_{\rm PV} = 1.5$ for Fig. 2 (a) and $H_{\rm PV} = 4.5$ for Fig. 2 (b) under the condition in Table I. It can be seen that the smaller $C_{\rm DC}$ and larger $H_{\rm PV}$ increase the nonlinearity of $V_{\rm DC}^*$ function (9).

TABLE I
Parameters for 6-bus Simulation

| | Item | Specification |
|---|---|---|
| | Inertia coefficient of SG | 3 |
| | Inertia coefficient of DFIGs | 1.5 |
| | Terminal bus voltage | 25 kV |
| | Output voltage | 4160 V |
| PV | DC-link nominal voltage | 6500 V |
| systems | DC-link voltage boundary | ± 200 V |
| | DC-link capacitance | 5 mF |

Generally, the lower limit of the DC-link voltage can be set to avoid over-modulation of the VSC, the upper limit is the maximum rated voltage of physical capacitor. If a high nominal voltage is used, more energy will be available for inertia emulation. However, using high voltage will bring in many problems. First, it will increase switching harmonic distortion, which requires bulky output filters. Second, it will increase switching loss and lower system efficiency. Third, voltage rating of other components is needed to match the voltage setting. To avoid these problems, we only consider normal value and narrow DC-link voltage ranges.

In order to reduce computational complexity, (9) can be simplified due to the narrow DC-link voltage ranges. The derivative of (9) at $f_0$ can be obtained as

$$\dot{V}_{\rm DC}^*|_{f0} = \frac{2 H_{\rm PV} S_{\rm PV}}{C_{\rm DC} f_0 V_{\rm DC0}}. \tag{10}$$

Through linearization, the equation for DC-link voltage reference can be simplified according to (11)

$$V_{\rm DC}^* = \frac{2 H_{\rm PV} S_{\rm PV}}{C_{\rm DC} f_0 V_{\rm DC0}} (f - f_0) + V_{\rm DC0}. \tag{11}$$

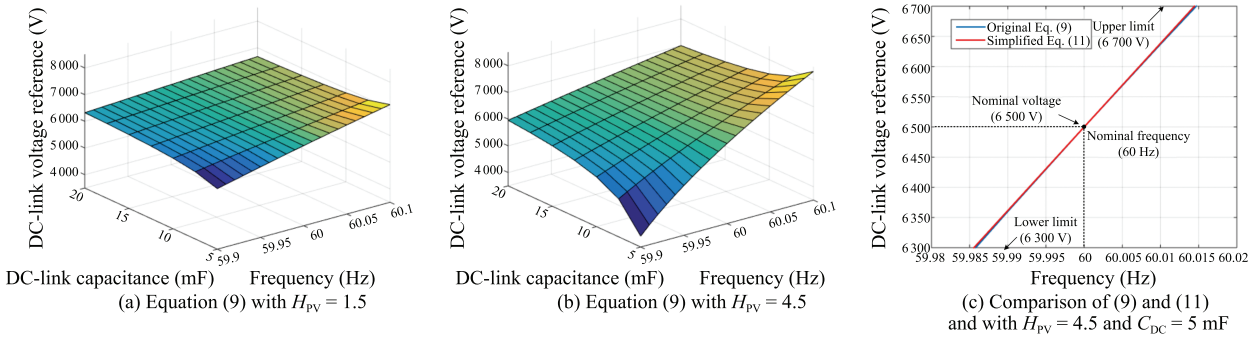


(a) Equation (9) with $H_{PV} = 1.5$ (b) Equation (9) with $H_{PV} = 4.5$ (c) Comparison of (9) and (11) and with $H_{PV} = 4.5$ and $C_{DC} = 5$ mF

Fig. 2. Relationship between voltage reference, DC-link capacitance, frequency, and inertia time constant.

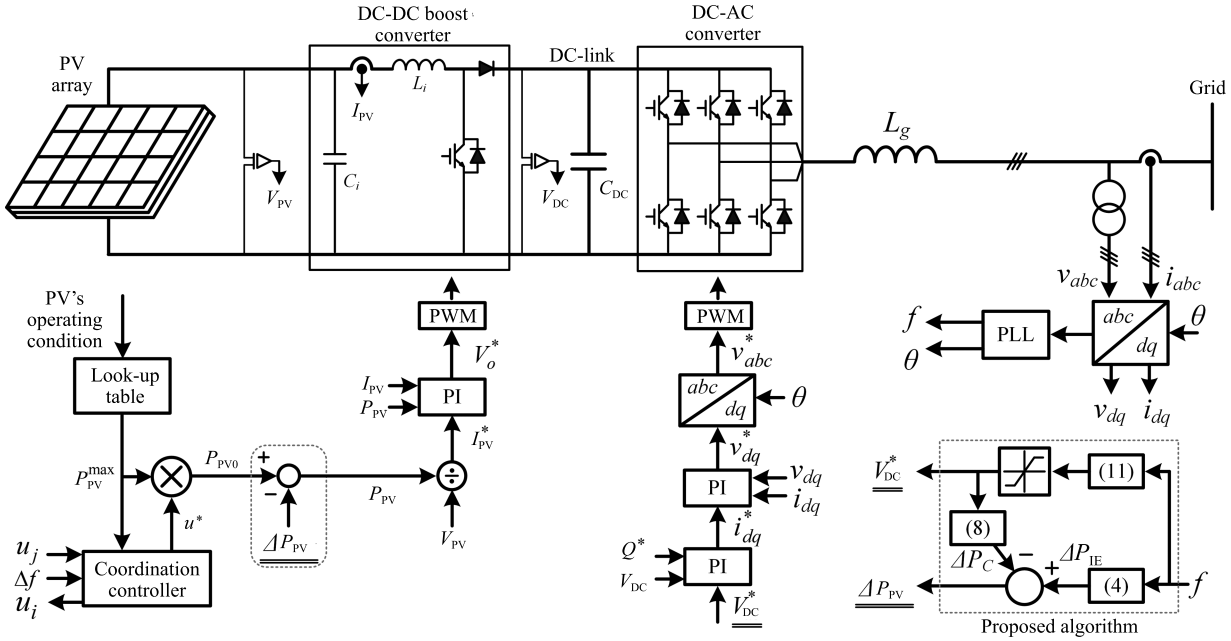


Fig. 3. Overall block diagram of the proposed virtual inertia based control strategy.

By comparing (11) with (9), it can be seen that the original nonlinear function with respect to f is transformed into a simple linear function. As shown in Fig. 2 (c), the difference between the nonlinear and linear relationships is very small due to the limited operating range. Thus, (11) is a better choice than (9) due to its good balance of accuracy and simplicity.

### *B. Inertia Emulation Through PV Array Generation Adjustment*

The PV array's generation setting ($P_{\rm PV}$) can be calculated according to (12).

$$P_{\rm PV} = P_{PV0} - \Delta P_{\rm PV} = P_G + \Delta P_C. \tag{12}$$

It should be noted that the $P_{\rm PV}$ calculated according to (12) has already considered the overall requirement for inertia emulation. Even though $\Delta P_{\rm PV}$ is not directly calculated based on $\Delta P_{\rm PV} = \Delta P_{\rm IE} - \Delta P_C$, (12) can make sure the desired $P_G$ is generated.

### *C. Algorithm Implementation*

Fig. 3 shows the overall block diagram of the proposed virtual inertia based control strategy. First, PV array's maximum generation $P_{\rm PV}^{\rm max}$ is estimated according to the PV array's operating condition. Based on microgrid's overall generation capability and demand, the utilization level $u^*$ is updated by the upper-level controller, which could be either centralized or fully distributed [16]−[17]. Based on $P_{\rm PV}^{\rm max}$ and $u^*$, $P_{G0}$ ($P_{PV0}$) can be calculated. During steady state, there is no need for inertia emulation ($\Delta P_{\rm IE} = 0$). Thus, $P_{G0}$ will be used as control reference for the DC-DC boost converter and the nominal DC-link voltage ($V_{\rm DC0}$) will be used as reference for DC-AC converter control.

During transient states, the proposed virtual inertia control algorithm is activated. The calculations of $\Delta P_{\rm PV}$ and $V_{\rm DC}^*$ for inertia emulation are illustrated in Fig. 4. First, the total amount of power required for inertia emulation ($\Delta P_{\rm IE}$) is calculated according to (4). Based on parameter setting and frequency, $V_{\rm DC}^*$ can be calculated according to (11). According to $V_{\rm DC}^*$, the amount of power for inertia emulation covered by the DC-link capacitor ($\Delta P_C$) can be calculated according to (8). By subtracting $\Delta P_C$ from $\Delta P_{\rm IE}$, $\Delta P_{\rm PV}$ can be calculated. Finally, the adjusted $V_{\rm DC}^*$ and adjustment to $P_{\rm PV}$ are obtained for virtual emulation. The updated values are used as control references for the DC-DC boost converter and DC-AC inverter, respectively.

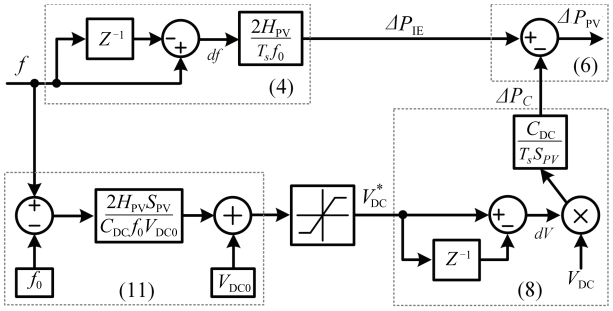


Fig. 4. Calculation of PPV and $V^*_{\rm DC}$ for inertia emulation.

This proposed virtual inertia control algorithm is suitable for autonomous microgrids with PV systems. In grid-connected mode of the microgrid, since sufficient inertia is provided by the main power grid, there is no need for inertia emulation within the microgrid. If the PV systems are operated at the MPPT mode, there is no extra power requirement for inertia emulation. If a microgrid is operating autonomously, the PV systems may not work at the MPPT mode when available renewable generation is more than needed. Even if there is no surplus renewable generation, the PV systems could run at deloading mode, which creates concerns on stability and transient performance outweighing the concern on energy efficiency. The existence of generation margin due to deloading allows the imposing of the presented virtual inertia control strategy. The first option of DC-link voltage control is only capable of damping slight frequency oscillations yet can reduce impact in PV array side. The second option of PV array generation adjustment is much more capable and can accommodate all the remaining demand for inertia emulation.

## IV. Simulation Studies

During simulation studies, the proposed virtual inertia based control strategy is integrated with the gradient-based distributed coordination algorithm [17] and tested with a 6-bus renewable microgrid shown in Fig. 5. The microgrid contains 6 loads, three DFIGs, two PVs and one SG. The DFIG at bus-1 (abbreviated as DFIG1) is controlled in reactive power regulation mode, the DFIG4 and DFIG5 are controlled in voltage regulation mode, and the PV2 and PV3 are controlled in unit power factor mode. The active power output of the SG is maintained at zero when the wind power is sufficient. When the wind power is insufficient, the SG is controlled to increase the output for regulating the frequency. The ramp-up and ramp-down rates of the SG are both set to be 0.4 MW/s. During simulations, time step for utilization level update is selected to be 0.1 s, which has good balance of control performance and technical feasibility. More information about the distributed algorithm and the 6-bus microgrid model can be found in [17].

The wind speeds of the DFIGs at bus-1, bus-4, and bus-5 are constant at 11 m/s, 14 m/s, and 14 m/s, respectively. The solar insolation of PVs at bus-2 and bus-3 are 900 w/m$^2$ and 1000 w/m$^2$, respectively. Hence, the available renewable generation active power are 1.95, 4,05, 4.50, 6.00, and 8.50 MW. The active loads are 5.00, 3.00, 6.00, 3.00, 2.00 and 4.00 MW, and the inductive loads are 1.00, 0.80, 1.20, 0.60, 0.80 and 2.00 MVar, respectively. The SG's initial generation power in

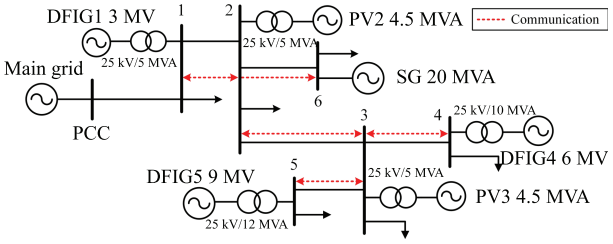


Fig. 5. Single line diagram of a 6-bus microgrid and communication topology.

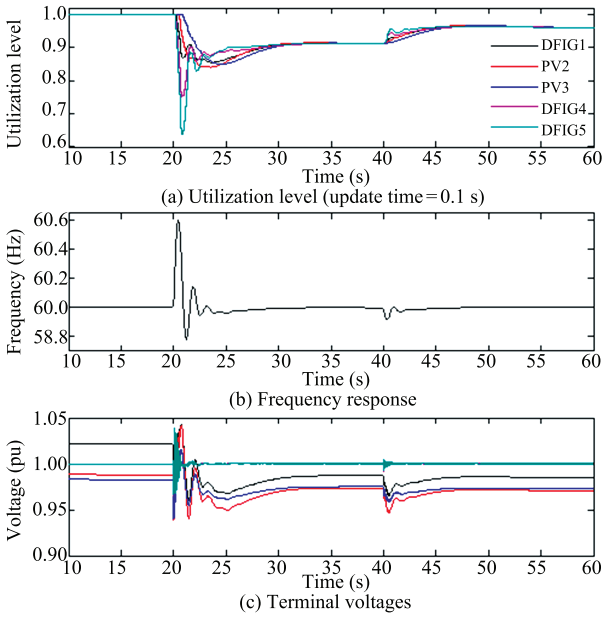


Fig. 6. System responses without the proposed algorithm.

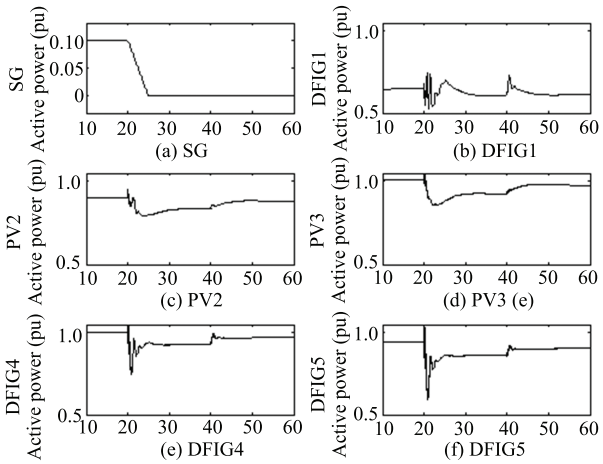


Fig. 7. Active power of five RGs without the proposed algorithm.

the grid-connected mode is 2 MW. An islanding event at 20 s and 5 % load increase event at 40 s are simulated to test and compare the performance of the proposed control.

The results without the proposed algorithm are shown in Figs. 6 and 7. Before 20 s, the microgrid operates in grid-connected mode so that all the utilization levels in Fig. 6 (a) are maximum value 1 which means that all RGs are using MPPT control. The terminal voltages of DFIG4 and DFIG5 are controlled on the nominal value by voltage regulation mode, and the other terminal voltages are placed around the nominal

value without large errors as shown in Fig. 6 (c). In Fig. 7, The output power of the SG and five RGs present the available maximum $P_{\mathrm{PV}}^{\max}$ and initial values. Since the total power of RGs is larger than the sum of microgrid loads, the rest of the power is transmitted to the main grid through PCC.

After 20 s, the distributed coordination control is activated by the algorithm of [17]. Then the utilization levels are changed to satisfy the supply-demand balance in the islanding mode. In Fig. 6 (b), the peak value of the frequency deviation is about 0.6 Hz. All the active power outputs of RGs in Fig. 7 track well the common references in Fig. 6 (a). After islanding mode, the total power generation is sufficient to satisfy the microgrid loads. Thereby the active power of the SG goes down toward zero in 5 s in Fig. 7 (a). All the waveforms can be converged in 40 s.

Then, the 5 % load increase occurs at 40 s. By using the distributed coordination control, the new utilization levels are conveyed. The frequency is converged after short transient time. In the case of 5 % load increase, the maximum frequency deviation is approximately 0.08 Hz.

Figs. 8 and 9 show the results with the proposed virtual inertia algorithm. In the simulation, the inertia coefficients $H_{\mathrm{PV}}$ of two PVs are both 1.5. After the islanding event, even though the minimum value of the utilization levels is higher than that of Fig. 6 (a), the frequency deviation is reduced approximately 0.1 Hz as shown in Fig. 8 (b). In the case of the load increase, the frequency deviation is improved about 0.01 Hz. The output powers of three DFIGs in Fig. 9 are nearly similar to those of Fig. 7. However, the two PV's outputs are different due to the proposed algorithm. The zoomed and overlaid system responses with and without the presented inertia emulation (IE) strategy are presented in Fig. 10. The improvement of the frequency damping can be confirmed through Fig. 10 (a). The output active power revised by the proposed algorithm are shown in Figs. 10 (b) and 10 (c). In the case without algorithm, the two active powers of PVs are just tracking the utilization level after islanding mode. In the

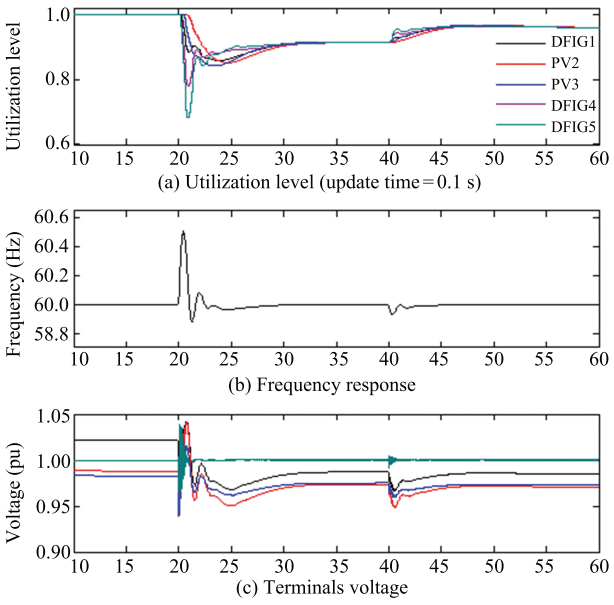


Fig. 8. System response with the proposed algorithm ($H_{\mathrm{PV}} = 1.5$).

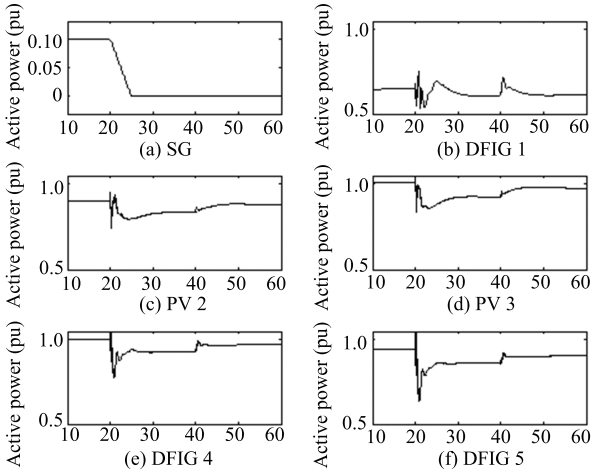


Fig. 9. Active power of 5 RGs with the proposed algorithm ($H_{\mathrm{PV}} = 1.5$).

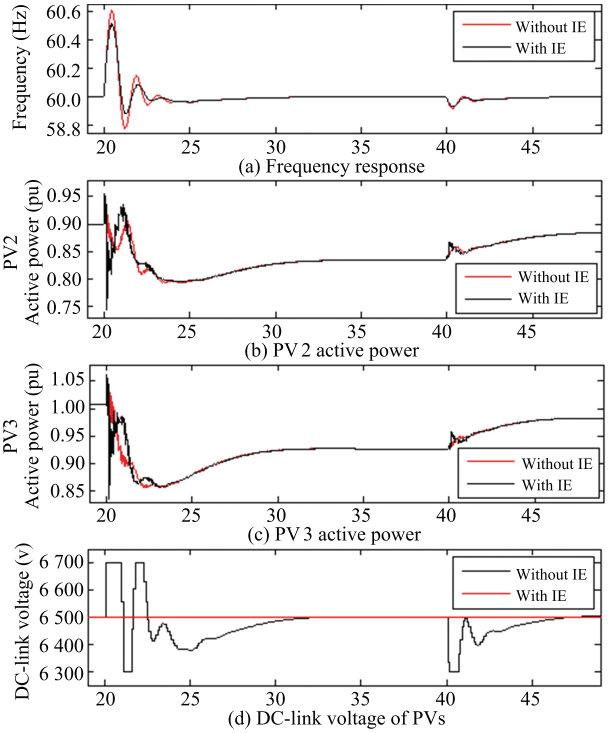


Fig. 10. Zoomed and overlaid waveforms.

case with the algorithm, however, the active powers calculated by the proposed algorithm are added to reference power $P_{G0}$ for emulating inertia. When the frequency increases, the active powers of PVs decrease. In contrary, when the frequency decreases, the active powers increase. As a result, the frequency deviation can be reduced. As shown in Fig. 10 (d), the DC-link voltage varies according to the frequency so that the charging or discharging power help the frequency to be stable. In particular, when the frequency deviation is small, all the power $\Delta P_{\mathrm{IE}}$ can be covered by the DC-link capacitor without any support from PV array. It means that the DC-link capacitor is acting as a good buffer to avoid the frequent reference change in PV array.

In the previous test, the update time of the reference setting $P_{G0}$ from upper level controller is 0.1 s due to the consideration of the system stability. However, after adding

the proposed virtual inertia, the system can have decent time to control. Even though the global reference $P_{G0}$ is updated slowly, the local reference $\Delta P_{\rm IE}$ for inertia emulation can be changed itself. Thus, the system can be stable although the update time is large. The results with a large update time 0.3 s are shown in Figs. 11 and 12. The utilization level $u^*$ i.e., power reference $P_{G0}$ is updating every 0.3 s as shown in Fig. 11 (a). In spite of the disconnection form the grid at 20 s or 5 % load increase change at 40 s, the system can be controllable to satisfy the supply-demand balance. Actually, it is because of the increased system inertia. In this test, inertia coefficient $H_{\rm PV}$ for two PVs are both 4.5. If the two inertia coefficients are lower than 4, the system becomes unstable after 20 s. As shown in Figs. 12 (c) and 12 (d), the two PV systems are generating the active powers based on the virtual inertia algorithm so that it can prevent frequency collapse. Therefore, the proposed virtual inertia control can help stabilizing system when the upper-level control reference cannot be delivered frequently enough.

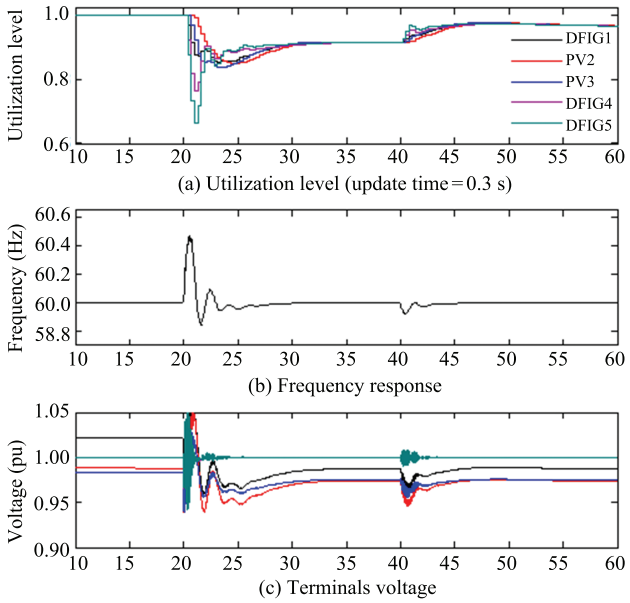


Fig. 11. System response with the proposed algorithm ($H_{\rm PV} = 4.5$).

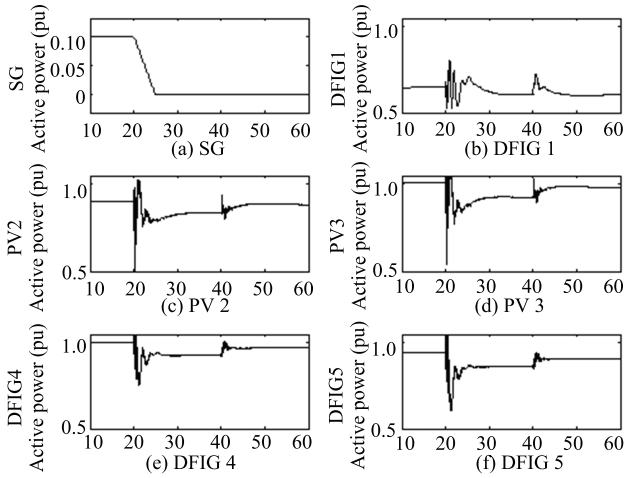


Fig. 12. Active power of 5 RGs with the proposed algorithm ($H_{\rm PV} = 4.5$).

## V. Conclusion

This paper presents a virtual inertia control strategy for PV systems in autonomous microgrid. The basic idea is to adjust generation based on a simplified SG model. The increasing or decreasing PV system generation is realized by adjusting the DC-link voltage and PV array output. By integrating the proposed solution with a previously developed distributed gradient-based coordination algorithm, transient performance can be improved and the demanding requirement on updating frequency can be relaxed. The solution is suitable for autonomous microgrids when they have surplus renewable generation and when consideration on transient performance outweighs energy efficiency. The basic idea can be extended to other types of RGs with DC-link capacitors. The solution tries to make microgrid work like a large power grid with large inertia. Thus, it cannot unlock the potentials of power electronics based microgrid in terms of flexibility and fast response. Future work should be focused on designing advanced fast and accurate microgrid controllers.

## References

[1] N. Hatziargyriou, H. Asano, R. Iravani, and C. Marnay, "Microgrids," *IEEE Power Energ. Magaz.*, vol. 5, no. 4, pp. 78−94, Jul.−Aug. 2007.

[2] N. Hatziargyriou, "Microgrids [guest editorial]," *IEEE Power Energ. Magaz.*, vol. 6, no. 3, pp. 26−29, May−Jun. 2008.

[3] G. Venkataramanan and C. Marnay, "A larger role for microgrids," *IEEE Power Energ. Magaz.*, vol. 6, no. 3, pp. 78−82, May−Jun. 2008.

[4] J. M. Guerrero, J. C. Vsquez, J. Matas, M. Castilla, and L. G. de Vicuña, "Control strategy for flexible microgrid based on parallel line-interactive UPS systems," *IEEE Tran. Ind. Elec.*, vol. 56, no. 3, pp. 726−736, Mar. 2009.

[5] J. Ekanayake and N. Jenkins, "Comparison of the response of doubly fed and fixed-speed induction generator wind turbines to changes in network frequency," *IEEE Tran. Energ. Conv.*, vol. 19, no. 4, pp. 800−802, Dec. 2004.

[6] A. Mullane and M. OMalley, "The inertial response of induction-machine-based wind turbines," *IEEE Tran. Power Syst.*, vol. 20, no. 3, pp. 1496−1503, Aug. 2005.

[7] G. Lalor, A. Mullane, and M. O'Malley, "Frequency control and wind turbine technologies," *IEEE Tran. Power Syst.*, vol. 20, no. 4, pp. 1905−1913, Nov. 2005.

[8] J. Morren, S. W. H. de Haan, W. L. Kling, and J. A. Ferreira, "Wind turbines emulating inertia and supporting primary frequency control," *IEEE Tran. Power Syst.*, vol. 21, no. 1, pp. 433−434, Feb. 2006.

[9] P. K. Keung, P. Li, H. Banakar, and B. T. Ooi, "Kinetic energy of wind-turbine generators for system frequency support," *IEEE Tran. Power Syst.*, vol. 24, no. 1, pp. 279−287, Feb. 2009.

[10] J. F. Conroy and R. Watson, "Frequency response capability of full converter wind turbine generators in comparison to conventional generation," *IEEE Trans. Power Syst.*, vol. 23, no. 2, pp. 649−656, May 2008.

[11] M. Kayikci and J. V. Milanovic, "Dynamic contribution of dfig-based wind plants to system frequency disturbances," *IEEE Trans. Power Syst.*, vol. 24, no. 2, pp. 859−867, May 2009.

[12] Z. X. Miao, L. L. Fan, D. Osborn, and S. Yuvarajan, "Wind farms with HVdc delivery in inertial response and primary frequency control," *IEEE Trans. Energ. Conv.*, vol. 25, no. 4, pp. 1171−1178, Dec. 2010.

[13] X. R. Zhu, Y. Wang, L. Xu, X. Y. Zhang, and H. M. Li, "Virtual inertia control of DFIG-based wind turbines for dynamic grid frequency support," *Proc. IET Conf. Renewable Power Generation*, Edinburgh, UK, 2011, pp. 1−6.

[14] J. B. Zhu, C. D. Booth, G. P. Adam, A. J. Roscoe, and C. G. Bright, "Inertia emulation control strategy for VSC-HVDC transmission systems," *IEEE Tran. Power Syst.*, vol. 28, no. 2, pp. 1277−1287, May 2013.

[15] G. Delille, B. François, and G. Malarange, "Dynamic frequency control support by energy storage to reduce the impact of wind and solar generation on isolated power systems Inertia," *IEEE Tran. Sustain. Energ.*, vol. 3, no. 4, pp. 931−939, Oct. 2012.

[16] W. Zhang, Y. L. Xu, W. X. Liu, F. Ferrese, and L. M. Liu, "Fully distributed coordination of multiple DFIGs in a microgrid for load sharing," *IEEE Tran. Smart Grid*, vol. 4, no. 2, pp. 806−815, June. 2013.

[17] Y. L. Xu, W. Zhang, W. X. Liu, X. Wang, F. Ferrese, C. Z. Zang, and H. B. Yu, "Distributed subgradient-based coordination of multiple renewable generators in a microgrid," *IEEE Tran. Power Syst.*, vol. 29, no. 1, pp. 23−33, Jan. 2014.

**Won-Sang Im** received the B.S., M.S. and Ph.D. degrees in electrical computer engineering from Pusan National University, Busan, in 2007, 2009, and 2013, respectively. He is currently a postdoctoral researcher at Lehigh University, Bethlehem, PA, USA. His research interests include electric machine drives, power conversion system, microgrid, their diagnosis and tolerance controls.

**Cheng Wang** received the B.S. degree in electrical engineering from Southwest Jiaotong University, China in 2011, and is currently working toward the Ph.D. degree in electrical engineering at the School of Electrical and Electronics Engineering, Huazhong University of Science and Technology at Wuhan, China. He is also a research assistant with the Department of Electrical and Computer Engineering, Lehigh University at PA, USA. His research interests include high penetrative grid-interactive photovoltaic system, microgrid, modular multilevel converters, paralleled uninterrupted power supplies and flexible AC transmission system.

**Wenxin Liu** received the B.S. degree in industrial automation, and the M.S. degree in control theory and applications from Northeastern University, Shenyang, China, in 1996 and 2000, respectively, and the Ph.D. degree in electrical engineering from the Missouri University of Science and Technology (formerly University of Missouri CRolla), Rolla, MO, USA, in 2005. Then, he worked as an assistant scholar scientist with the Center for Advanced Power Systems, Florida State University, Tallahassee, FL, USA, till 2009. From 2009 to 2014, he was an assistant professor with the Klipsch School of Electrical and Computer Engineering, New Mexico State University, Las Cruces, NM, USA. Currently, he is an assistant professor with the Department of Electrical and Computer Engineering, Lehigh University, Bethlehem, PA, USA. His research interests include power systems, power electronics, and controls.

**Liming Liu** received the B.S. and M.S. degrees in electrical engineering from Wuhan University, China, in 1998 and 2003, respectively, and the Ph.D. degree in electrical engineering from Huazhong University of Science and Technology, China, in 2006. He joined the Center for Advanced Power Systems, Florida State University, Tallahassee, FL, USA, in 2007 as a postdoctoral researcher, where he was an assistant scientist from 2008 to 2013. He is currently a senior scientist at ABB Inc., Raleigh, NC, USA. His research interests generally include medium/high voltage DC voltage converter, modeling and control of multilevel inverter applications, renewable energy conversion systems, high penetrative grid-interactive photovoltaic system, smart grid, motor drive control with hybrid energy storages, and flexible AC transmission system.

**Jang-Mok Kim** received the B.S. degree from Pusan National University (PNU), Busan, Korea, in 1988; and the M.S. and Ph.D. degrees from the Department of Electrical Engineering, Seoul National University (SNU), Seoul, Korea, in 1991 and 1996, respectively. From 1997 to 2000, he was a senior research engineer with the Korea Electrical Power Research Institute (KEPRI), Daejeon, Korea. Since 2001, he has been with the School of Electrical Engineering, PNU, where he is presently a Research Member in the Research Institute of Computer Information and Communication, a Faculty Member, and a head of the LG Electronics Smart Control Center. As a visiting scholar, he joined the Center for Advanced Power Systems (CAPS), Florida State University, Tallahassee, Florida, in 2007. His current research interests include the control of electric machines, electric vehicle propulsion, and power quality.